The dithiol-dithione tautomerism of 2,3-pyrazinedithiol in the synthesis of copper and silver coordination compounds

Henfling, S.; Kempt, R.; Klose, J.; Kuc, A. B.; Kersting, B.; Krautscheid, H.;

Originally published:

October 2020

Inorganic Chemistry 59(2020)22, 16441-16453

DOI: https://doi.org/10.1021/acs.inorgchem.0c02203

The dithiol-dithione tautomerism of 2,3-pyrazinedithiol in the synthesis of copper and silver coordination compounds

Stefan Henfling, Roman Kempt, Jennifer Klose, Agnieszka Kuc, Berthold Kersting, Harald Krautscheid*

Abstract

A promising strategy for new electrically conductive coordination polymers is the combination of d^{10} metal ions, which tolerate short metal···metal distances, with dithiolene linkers, known for their "non-innocent" redox behavior. This study explores the coordination chemistry of 2,3-pyrazinedithiol (H_2pdt) towards Cu^+ and Ag^+ ions, highlighting similarities and differences. The synthetic approach, starting with the fully protonated ligand, allowed the isolation of a homoleptic bis(dithiolene) complex with formal Cu^I atoms, [Cu(H_2pdt)$_2$]Cl (**1**). This complex was further transformed to a one-dimensional coordination polymer with short metal···metal distances, ^{1D}[Cu(Hpdt)] (**2^{Cu}**). The larger Ag^+ ion directly built up a very similar coordination polymer ^{1D}[Ag(Hpdt)] (**2^{Ag}**), without any appearance of an intermediate metal complex. The coordination polymer ^{1D}[Cu(H_2pdt)I] (**4**), like complex **1**, bears fully protonated H_2pdt ligands in their dithione form. Upon heating, both compounds underwent auto-oxidation coupled with a dehydrogenation of the ligand to form the open shell neutral copper(II) complex [Cu(Hpdt)$_2$] (**3**) and the coordination polymer ^{1D}[Cu_2I_2(Hpdt)(H_2pdt)] (**5**), respectively. For all presented compounds, crystal structures are discussed in-depth. Furthermore, properties of **1**, **3**, as well as of the three one-dimensional coordination polymers **2^{Ag}**, **2^{Cu}** and **4**, were investigated by UV-Vis-NIR spectroscopy, cyclic voltammetry, and variable temperature magnetic susceptibility, and DC-conductivity measurements. The experimental results are compared and discussed with the aid of DFT simulations.

Introduction

Since the early 1960s, transition metal dithiolenes have become of great interest due to their unique electrochemical, spectroscopic, and magnetic properties.[1] They are ever more relevant to fields including photo-catalysis,[2] solar cells,[3–7] electrical and magnetic materials,[8–10] non-linear optics,[11,12] bioinorganic chemistry,[13,14] and photo catalysis for H_2 production.[15–18] Strong interactions between the metal atoms and ligands originate in a large overlap of the ligand and metal orbitals.[1,19,20] As a result, the corresponding molecular orbitals display a high degree of delocalization, suggesting that the ligand participates in the complex redox reaction.[1,20–22] The term "non-innocent" has been coined to describe this behavior. This is in contrast to "well-behaved" ligands, that allow, according to Jørgensen[23], the exact definition of the metal oxidation state. In recent years, particular effort has been devoted to enriching this class of compounds with nitrogen containing heterocyclic dithiolenes. 2,3-Pyrazinedithiol (H_2pdt) can be cited as one of the most exploited ligands. Rhenium and molybdenum oxo bis(pyrazine-dithiolene) complexes, for example, have been synthesized as structural models for the active sites of bacterial molybdenum cofactor containing enzymes.[24] As nitrogen in amines can act as Brønsted base, the nickel, palladium, and platinum pyrazine-dithiolene complexes have been studied for their proton-dependent electron transfer.[25–27] In addition, the nitrogen atoms have been exploited as additional donor atoms to construct frameworks with alkali metal ions,[28,29] as well as porous three-dimensional frameworks. With copper ions, the coordination networks Cu[Cu(pdt)$_2$] and Cu[Ni(pdt)$_2$] exhibit increased electrical conductivity.[8,30]

A common first step in synthesizing dithiolene complexes is the generation of the two-fold negatively charged dithiolate anion, typically through deprotonation of the corresponding dithiolene ligand. In a second step, the dithiolate is reacted with mostly di-, tri-, or tetravalent metal ions to obtain the corresponding complexes.[1,31] In this work, the main focus lies on one particular aspect of H_2pdt, its prototropic dithiol-dithione tautomerism. Katritzky et al.[32] discussed the movement of protons between a ring nitrogen atom and an atom adjacent to the ring. Since the UV-Vis-spectrum of pyrazine-2-thione is different from that of 2-methylthio-pyrazine, pyrazine-2-thione would likely exist in the thione form rather than in its thiol tautomer.[32] In the solid state, the N-H tautomeric form of H_2pdt is preferred as evidenced by the crystal structure analysis of H_2pdt (SI, section 5.3). All these findings suggest that H_2pdt might not necessitate any prior deprotonation step in order to synthesize S-donor coordination compounds. Considering that dithiones (charge ±0) are softer Lewis bases than dithiolates (2–) according to the HSAB concept and prefer coordination to soft metal ions,[33] the coordination chemistry towards monovalent d^{10} copper and silver ions was explored. We present the homoleptic formal Cu^I bis(dithiolene) complex and three one-dimensional coordination polymers and show, how these materials, highly susceptible to oxidation and deprotonation, can act as precursors for the open shell complex and coordination polymer [Cu(Hpdt)$_2$] (**3**) and ^{1D}[Cu_2I_2(Hpdt)(H_2pdt)] (**5**), respectively. The compounds are characterized by NMR spectroscopy and X-ray structure analysis. Their electronic properties are revealed via cyclic voltammetry, UV-Vis-NIR spectroscopy, DFT calculations, magnetic and electrical conductivity measurements.

Results and Discussion

Synthesis

H_2pdt was synthesized via a standard nucleophilic aromatic substitution reaction of 2,3-dichloropyrazine with NaSH, according to the literature.[19,29,30] H_2pdt was employed as a ligand for synthesis of Cu^I and Ag^I coordination compounds (Scheme 1), phase purity of these products was confirmed via powder X-ray diffraction (Figure SI-2). Those compounds that bear a fully protonated H_2pdt ligand underwent spontaneous oxidative dehydrogenation upon heating to form open shell Cu^{II} species.

Polymeric ^{1D}[Ag(Hpdt)] (**2^{Ag}**) was obtained directly in large scale under reflux conditions by reaction of H_2pdt with Ag_2SO_4 in methanol. In contrast to the reaction of Ag^+ ions with H_2pdt, leading directly to the insoluble, orange precipitate of **2^{Ag}**, the methanolic solution of Cu^+ ions with H_2pdt was dark blue, indicating the formation of a reaction intermediate. The ^{1}H NMR spectrum revealed one sharp singlet at 7.29 ppm and a broad one at around 15 ppm (Figure SI-1). This information already points towards a diamagnetic complex, bearing

one or more acidic protons. Single crystal X-ray diffraction reveals the structural details of the dark blue Cu^{I} complex [Cu(H$_2$pdt)$_2$]Cl (**1**).

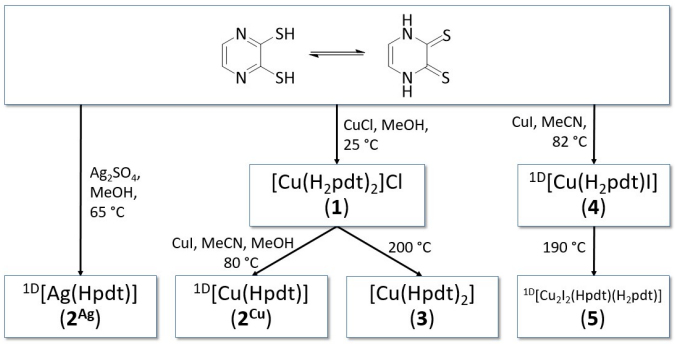

Scheme 1. Reaction scheme for the coordination compounds **1**–**5**.

The one-dimensional coordination polymer ^{1D}[Cu(Hpdt)] (**2^{Cu}**) was prepared by further reaction of **1** with CuI in a mixture of acetonitrile and methanol under mild hydrothermal conditions. All attempts to directly synthesize **2^{Cu}** from H$_2$pdt and one equivalent of Cu$^+$ ions led to the additional formation of the byproduct [Cu(Hpdt)$_2$] (**3**).

The reaction of H$_2$pdt with CuI in acetonitrile under reflux yielded the coordination polymer ^{1D}[Cu(H$_2$pdt)I] (**4**). The choice of the solvent was crucial for obtaining the desired product. Whereas CuI is easily soluble in acetonitrile, the solubility of H$_2$pdt is rather poor. Choosing a solvent with reversed solubilities of the starting materials, such as methanol, led again to dark blue solutions of the Cu^{I} complex [Cu(H$_2$pdt)$_2$]$^+$.

As indicated above, the fully protonated ligand H$_2$pdt facilitated the oxidation of Cu^{I} species via dehydrogenation of the ligand. By heating to 200 °C, **1** decomposed to the paramagnetic planar Cu^{II} complex **3**. In methanol the decomposition process started much earlier, and few minutes at 140 °C were sufficient to fully oxidize the Cu^{I} complex. Heating **4** above 190 °C enabled the reaction to ^{1D}[Cu$_2$I$_2$(Hpdt)(H$_2$pdt)] (**5**) with two crystallographically different copper atoms in their oxidation states +I and +II.

According to temperature dependent X-ray diffraction experiments (Figure SI-3), **2^{Cu}** is stable up to 200 °C, its silver analogue **2^{Ag}** is starting to decompose at 190 °C. Both, complex **1** and coordination polymer **4**, show changes in their PXRD patterns upon heating attributable to chemical reactions. Whereas the transformation from **1** to **3** is rather sharp at 200 °C, the reaction of **4** to **5** needs more time and takes place between 170 and 190 °C. Both reaction products are very stable; **5** decomposes at 270 °C, **3** at 330 °C.

Crystal Structures

[Cu(H$_2$pdt)$_2$]Cl (**1**)

Layering a methanolic solution of [Cu(H$_2$pdt)$_2$]Cl with diethyl ether yielded two kinds of single crystals. The main phase, **1**, crystallizes in the monoclinic crystal system, the second phase, **1'**, in the triclinic crystal system. The molecular geometry of the complex in both structures is very similar, merely the packing is different. The following paragraph describes the crystal structure of **1**, that of **1'** is discussed in the SI (section 5.4). The crystal structure analysis confirms the formation of the homoleptic dithiolene complex [Cu(H$_2$pdt)$_2$]$^+$, in which the pyrazinedithiolene is fully protonated in its N-H tautomeric form. The asymmetric unit consists of one copper dithiolene complex cation and a separate chloride anion, which compensates the positive charge of the complex. Figure 1 shows the slightly distorted tetrahedral coordination of the Cu^{I} atom with the dihedral angle between S1/Cu1/S2 and S4/Cu1/S3 planes being 84.61(3)°. One of the ligands is bent out of the long axis of the complex, described by the torsion angle S3–Cu1–S4–C6 = 7.5(1)°, as illustrated in Figure 1b.

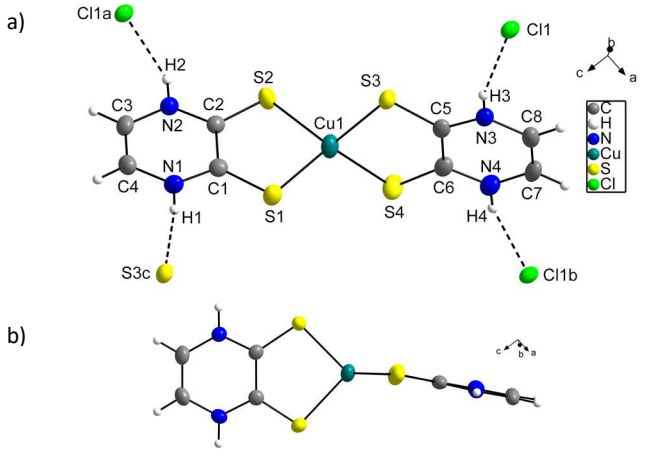

Figure 1. Ellipsoid representation (50 % probability ellipsoids) of the cation in [Cu(H$_2$pdt)$_2$]Cl (**1**) with N–H···Cl (306–312 pm) and N–H···S (333 pm) interactions (a) and depiction of the [Cu(H$_2$pdt)$_2$]$^+$ cation in viewing direction perpendicular to one ligand (b). Symmetry codes: a (1-x, 1-y, 1-z), b (2-x, -0.5+y, 0.5-z), c (x, y, 1+z).

The Cu–S distances are in the range of 227.70(8) to 231.72(9) pm (Table SI-3). They are slightly longer than in typical Cu^{II} dithiolene complexes and clearly longer than in typical Cu^{III} dithiolene complexes. The average Cu–S bond length in [Cu(qdt)$_2$]$^{2-}$ (qdt = quinoxaline-2,3-ditiholate), for instance, is 226(2) pm, in [Cu(pdt)$_2$]$^-$ it is 218.2(1) pm.[29,34] The increase in bond length upon reduction of copper dithiolene complexes from Cu^{III} to Cu^{II} has often been observed and described in the literature, and is in accordance with the molecular orbital scheme and the occupation of the LUMO, which is antibonding with respect to the Cu–S σ-bonds.[29,34] The interatomic distances in the H$_2$pdt ligand differ significantly from the deprotonated ligand in (Bu$_4$N)[Cu(pdt)$_2$][29]. In the copper(III) complex, the ligand can be considered as redox innocent dianion, stabilizing the copper atom in its +III oxidation state. Figure 2 illustrates that in the aromatic system of pdt^{2-}, all C–C and C–N distances tend to equalize and range between 133 and 141 pm, whereas in the protonated ligand in **1**, although formally aromatic, there is a clear difference in bond lenghts. They range from 134 to 147 pm and are very similar to those derived from the crystal structure analysis of the free ligand (chapter 5.3 in SI). The C–S bond lengths have often been used as indicator for the redox non-innocence of the dithiolene ligand. Sellmann et al.[35] synthesized the three complexes [Ni(LBu)$_2$]$^{0,1-,2-}$ (LBu^{2-} = 3,5-di-tert-butylbenzene-1,2-dithiolate) and characterized their electron bonding energies by XPS. They concluded that the ligand acts as "normal [innocent] 1,2-dithiolate ligand"[35] and that the redox processes take place mainly at the NiS$_4$ core of the complexes. C–S bond lengths considerations by Ray et al.,[21] however, declared the ligand to take part in the oxidation process, going from the dianionic to the neutral species, with the presence of one and two ligand *σ*-dithiosemiquinonate(1–) π-radicals in [Ni(LBu)(LBu·)]$^-$ and [Ni(LBu·)$_2$], respectively. They mainly emphasized the decrease in the average C–S bond length from 176.5, to 174.5, to 172.5 pm upon the two oxidation processes. In consideration of a much shorter average C–S distance in [Cu(H$_2$pdt)$_2$]$^+$ of 168.1(5) pm, none of the ligands is regarded as semiquinonate type π-radical, but rather as a completely oxidized dithione species.

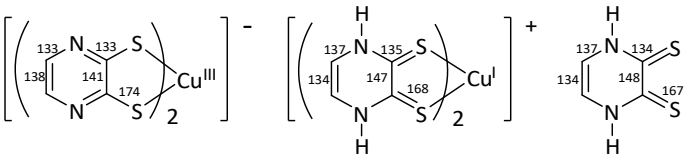

Figure 2. Average intraligand bond lengths in pm of pdt^{2-} in (Bu$_4$N)[Cu(pdt)$_2$][29], its protonated form [Cu(H$_2$pdt)$_2$]$^+$ in **1**, and in the free ligand, H$_2$pdt.

As shown in Figure 3, $[Cu(H_2pdt)_2]^+$ units are assembled to columns along [10$\bar{1}$] direction. The H_2pdt ligands of adjacent complexes display π···π interactions with 331 pm and 360 pm between parallel pyrazine rings. The shorter interactions involve the symmetry related H_2pdt ligands that are slightly tilted around S3 and S4, whereas the longer interactions are found between ligands with planar environment of the sulfur atoms S1 and S2. The columns, in turn, are linked directly via hydrogen bonds of H1 to S3 (N1···S3c = 332.9(3) pm) and indirectly via μ_3-Cl1 to H2, H3, and H4 (N···Cl = 306.4(3)–311.8(2) pm) (Table SI-1, Figures 1 and 4).

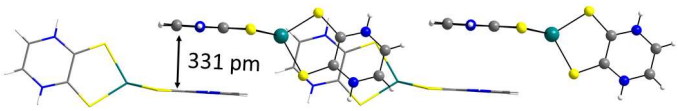

Figure 3. Representation of π···π stacking between complexes of **1** in one column, growing along [10$\bar{1}$]. The parallel pyrazine rings in the central part of the diagram are separated by 360 pm.

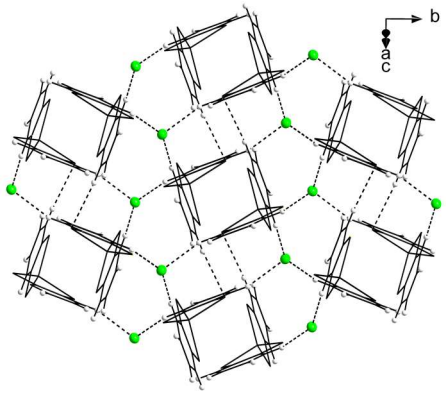

Figure 4. Interconnection of $[Cu(H_2pdt)_2]_n^{n+}$ columns via hydrogen bonding interactions.

In their 2003 book chapter about structures and structural trends in homoleptic dithiolene complexes, Beswick et al.[36] emphasized that there is no homoleptic Cu^I bis(dithiolene) described in the literature. The much softer dithione starting material, enabled by the thione thiol prototropic tautomerism, stabilizes this unusual oxidation state in the homoleptic dithiolene complex $[Cu(H_2pdt)_2]^+$. A similar stability for the formal oxidation state of +I in a tetrahedral CuS_4 coordination geometry was recently found in dithione complexes $[Cu(iPr_2Dt)_2]^+$ and $[Cu(Me_2Dt)_2]^+$ (iPr_2Dt = N,N′-diisopropyl-1,2-piperazine dithione, and Me_2Dt = N,N′-dimethyl-1,2-piperazine dithione).[37]

^{1D}[Ag(Hpdt)] (**2^{Ag}**) and ^{1D}[Cu(Hpdt)] (**2^{Cu}**)

Single crystals of **2^{Ag}** were obtained under solvothermal conditions. However, long time at high temperatures, required for the formation of crystals suitable for single crystal X-ray diffraction, also led to the decomposition of the ligand, and amorphous byproducts were formed besides the orange needles of the desired product. **2^{Ag}** crystallizes in space group $P2_1/n$, with one formula unit in its asymmetric unit. The formal $Hpdt^-$ monoanion acts as a μ_3-bridge and is connecting the metal atoms to a polymeric one-dimensional chain, as shown in Figure 5a. The Ag^I atom is coordinated by S1 and S2 of the chelating $Hpdt^-$ and by one sulfur atom S2a of a symmetry related $Hpdt^-$ ligand in a trigonal arrangement. The coordination is completed to trigonal pyramidal by a fourth sulfur atom, S1b, in apical position. All sulfur atoms are μ_2 coordinating, S2 is located on base edges of two pyramids around Ag1 and Ag1c (267.3(1) pm, 252.2(1) pm), and S1 is forming, in addition to one edge (252.8(1) pm), the top of a second pyramid with a significant larger Ag–S distance of 276.0(1) pm (Ag1–S1b). As a consequence, the Ag^I atoms are assembled to zig-zag chains with a Ag···Ag distance of 299.06(6) pm. This value is 45 pm shorter than the sum of the van der Waals radii.[38] The polymeric chains are oriented in *b* direction (Figure 5), and the close N···N distances (284.3(6) pm) between neighboring chains enable N–H···N hydrogen bonds between them. Between the one-dimensional coordination polymer chains, narrow pore channels of about 300 x 350 pm^2 account for a total potential solvent volume[39] of 16 %.

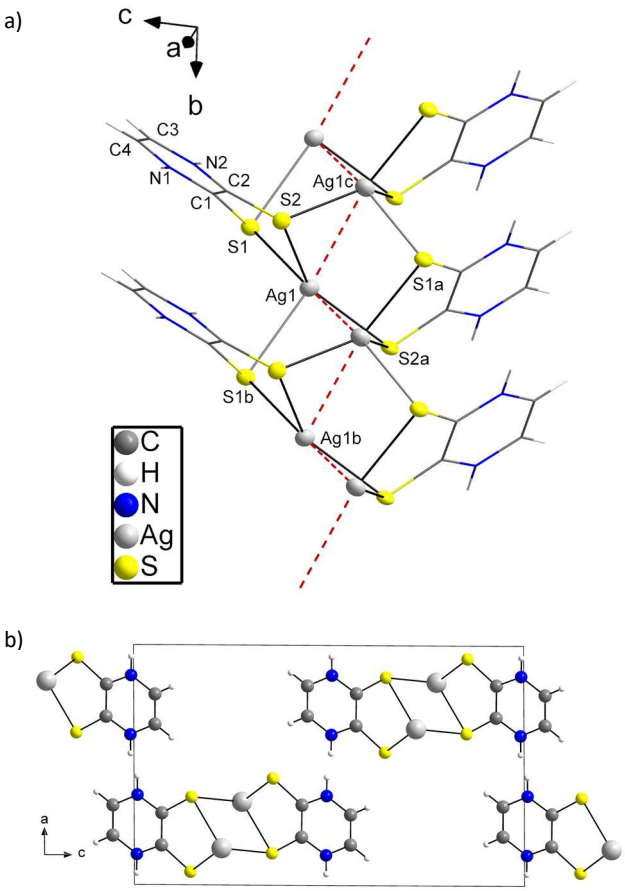

Figure 5. Fragment of a ^{1D}[Ag(Hpdt)] chain in **2^{Ag}** (a); N–H hydrogen atoms are disordered with 50 % occupancy; symmetry codes: a (0.5-x, 0.5+y, 0.5-z), b (x, 1+y, z), c (0.5-x, -0.5+y, 0.5-z). Packing of ^{1D}[Ag(Hpdt)] chains in **2^{Ag}**, view along [010] (b).

Table 1. Selected bond lengths (in pm) and angles (in °) in **2^{Ag}** and **2^{Cu}**.

Ag^I coordination in **2^{Ag}**		Cu^I coordination in **2^{Cu}**	
S1–Ag1	252.8(1)	S1–Cu1	224.4(3)
S2–Ag1	267.3(1)	S2–Cu1	226.8(3)
S2a–Ag1	252.2(1)	S2–Cu1b	222.4(3)
S1b–Ag1	276.0(1)	S1a–Cu1b	392.0(3)
S1–Ag1–S2	81.82(4)	S1–Cu1–S2	96.9(1)
Ag1a–S2a–Ag1	70.23(3)	Cu1–S2–Cu1b	72.88(8)
Ag1b–S1b–Ag1	101.28(4)	Cu1a–S1a–Cu1b	79.68(9)
Ag1b–Ag1a–Ag1	86.30(2)	Cu1a–Cu1–Cu1b	102.21(9)
$Hpdt^-$ in **2^{Ag}**		$Hpdt^-$ in **2^{Cu}**	
C1–S1	171.9(5)	C1–S1	171(1)
C2–S2	172.3(5)	C2–S2	176(1)
C1–C2	146.2(7)	C1–C2	146(2)
C1–N1	134.6(7)	C1–N1	133(1)
C2–N2	134.2(7)	C2–N2	134(1)
C4–N1	135.1(7)	C4–N1	137(1)
C3–N2	135.8(7)	C3–N2	134(1)
C3–C4	135.4(8)	C3–C4	136(2)

The structure motif of **2^{Cu}**, represented in Figure 6a, is very similar to its Ag analogue, though crystallizing in the polar space group $Pna2_1$. Another major difference is the trigonal planar coordination geometry of the copper atom with shorter Cu–S distances, ranging from

222.4(3) pm to 226.8(3) pm (Table 1). The smaller atom radius of the copper atom might preclude the additional coordination in apical position. As a result, the ligands are less rotated around their long axis, and the chain is more straight (∡(Cu Cu' Cu'') = 102.21(9)°) compared to **2**^{Ag} (∡(Ag Ag' Ag'') = 86.30(2)°). The Cu···Cu distance of 266.8(2) pm is 13 pm shorter than the sum of the van der Waals radii.[38] Calatayud et al.[40] described a similar structure with 1,2-dithiosquarate connecting Cu^{I} atoms to polymeric chains, bearing one negative charge per $[Cu(dtsq)]^{-}$ unit. The Cu^{I} atoms in $^{1D}[Cu(dtsq)]_n^{n-}$, however, display both trigonal planar and tetrahedral coordination geometry, with a relative large spread in the C–S bond distances of 225.1(1)–253.5(1) pm, the larger bonds involving sulfur atoms bridging three copper atoms. The intra-chain metal···metal distance of 266.8(2) pm, observed in **2**^{Cu}, lies in the range of the Cu···Cu distances in the anionic chain polymers of $^{1D}[Cu(dtsq)]_n^{n-}$ from 260.89(7) to 342.8(1) pm. As in **2**^{Ag}, the $^{1D}[Cu(Hpdt)]$ chains lie on twofold screw axes and are connected via N–H···N hydrogen bonds of N···N = 279(1) pm (Figure 6b). The hydrogen atom of the $Hpdt^{-}$ ligand in **2**^{Ag} is assumed to be disordered on both nitrogen atoms, N1 and N2, reflected in just a slight distortion (within standard uncertainty) of an ideal C_{2v} symmetry of the ligand. Both C–S distances are identical within one standard deviation (171.9(5) and 172.3(5) pm). In **2**^{Cu} the hydrogen atom is located on N1. The overall lowering in symmetry is mainly visible in the shortening of the adjacent C1–S1 bond to 171(1) pm, in contrast to 176(1) pm of C2–S2.

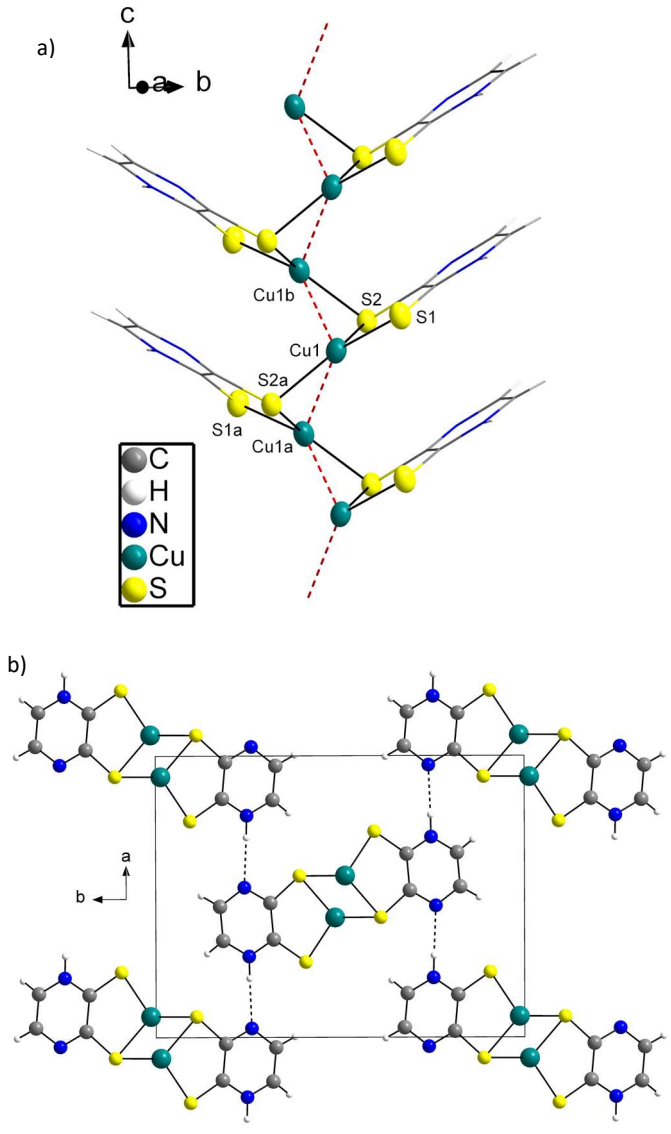

Figure 6. Fragment of a $^{1D}[Cu(Hpdt)]$ chain in **2**^{Cu} (a); symmetry codes: a (1-x, 1-y, -0.5+z), b (1-x, 1-y, 0.5+z). Packing of $^{1D}[Cu(Hpdt)]$ chains in **2**^{Cu} with N–H···H interactions (b).

M···M interactions in **2**^{Ag} and **2**^{Cu}

The question about possible interactions between formally closed shell d^{10} cations has been addressed in numerous works.[41–46] The usual, qualitative assignment of the M···M bonding in closed shell cations would result in a bond order of zero. Numerous cluster-like assemblies and complexes, however, with M···M distances of d^{10} cations much shorter than the sum of their van der Waals radii have been published and are described by the term of metallophilicity.[47] Early extended Hückel molecular orbital calculations suggested that there is a soft bonding interaction between the metal centers resulting from hybridization of the d orbitals with s and p shells and providing a surplus of occupied M···M bonding molecular orbitals.[41,42,48] Later, SCF-Xα-SW and DFT molecular orbital calculations of binuclear silver and copper complexes showed no significant involvement of p orbitals to the M···M bonding and, consequently, no attractive interaction.[43,44] The role of the ligand cannot be neglected in the interpretation of short M···M distances. Another explanation for such short M···M distances in bridged clusters is based on the nature of M–L–M three center bonding.[45,49] Systems with an acute M–L–M angle typically show shorter M···M distances than systems with larger M–L–M angle. This is explained with a closed three-center two-electron bond with attractive M···M interactions.[45,49] More recent literature demonstrates, that the metallophilic interactions between closed shell metal atoms are mainly based on the relativistic, and electron correlation effects.[46] Latter are comparable to van der Waals interactions, but may become unusually strong, and have been also described as "super van der Waals interactions".[50,51] In both **2**^{Ag} and **2**^{Cu}, the metal···metal distances are short with rather acute M–S–M bridging angles of 70°–73°. It is noteworthy that with the absolute value of the M···M distance in **2**^{Ag} being larger than in **2**^{Cu} (299.06(6) pm vs. 266.8(2) pm), it is shorter in proportion to the sizes of the van der Waals radii[38] (15 % shorter vs. 5 % in **2**^{Cu}). One reason might be the increasing relativistic effect as well as the additional Ag–S interaction, which leads to a compression of the polymer along its growth-axis. Even if the strength of the attractive forces is unclear, one could conclude that Ag^{I} atoms tolerate a shorter distance more easily in a comparable coordination environment.

$[Cu(Hpdt)_2]$ (**3**)

Heating **1** above 200 °C resulted in a complete and irreversible change of its X-ray diffraction pattern (Figure SI-4). Single crystals of the high temperature product were obtained via diffusion-controlled reaction of CuSCN with H_2pdt in methanol. The mechanism to form the formal open shell Cu^{II} complex may be described as oxidation with dehydrogenation of the ligand. Protonation of $[Ni/Pd/Pt(pdt)_2]^{-/2-}$ complexes have already been the subject of investigations for the effect upon electronic coupling within the molecule.[25,26] According to the X-ray crystal structure analysis, **3** crystallizes in space group $P\bar{1}$ with one formula unit per unit cell. The copper atom resides on an inversion center and is coordinated by two symmetry equivalent $Hpdt^{-}$ units in a square planar fashion (Figure 7). The average Cu–S bond length of 227.9(1) pm (Table SI-4) is similar to that of other Cu^{II} dithiolene complexes like $[Cu(qdt)_2]^{2-}$ (226(2) pm)[34]. As expected, the C–S bond lengths of, on average, 171.0(2) pm, are in between those of the pure dithiolate complex $[Cu(pdt)_2]^{-}$ (173.7(5) pm)[29] and those of the pure dithione form in **1** (168.1(5) pm). Since two equally strong electron density peaks were residing both near N1 and N2, the proton is regarded as disordered in the crystal structure refinement. This is also in accordance with the C–C and C–N distances, which are evenly distributed. Comparable to **2**^{Ag}, the ligand displays idealized C_{2v} symmetry. Figure 7b illustrates the complex, viewed parallel to the molecular plane; the dihedral angle between the CuS_4 unit and the pyrazine ring, 7.40(6)°, gives evidence for a small deviation from planarity. This chair conformation type distortion has been observed in some other diffraction studies of planar dithiolene complexes[28,29] and can be understood by looking at the packing of the complexes. As illustrated in Figure 8, they are regularly stacked in *a* direction with a

face to face distance of 337.4(2)–348.2(3) pm. Bending of the complex increases the intermolecular Cu···S interaction of neighboring complexes in one stack, reaching 324.41(7) pm.

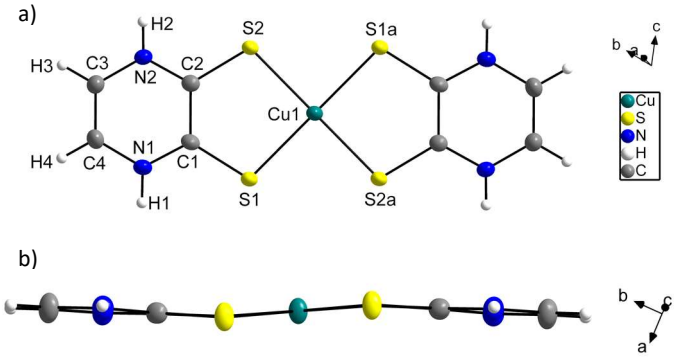

Figure 7. Ellipsoid representation (50 %) of $[Cu(Hpdt)_2]$ (**3**) in perpendicular (a) and parallel (b) views to the molecular plane. The hydrogen atom H1/H2 is disordered with site occupation factors of 0.5 each. Symmetry code: a (1-x, -y, 1-z).

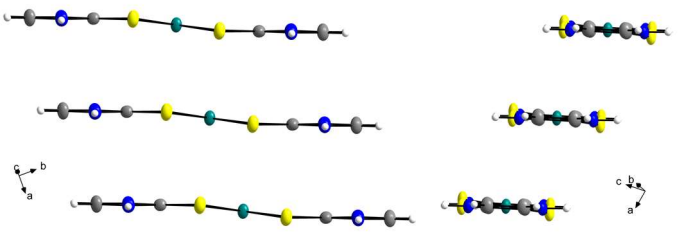

Figure 8. Stack of $[Cu(Hpdt)_2]$ moieties in **3**, viewed along their short (left) and long axis (right).

$^{1D}[Cu(H_2pdt)I]$ (**4**)

Compound **4** crystallizes in space group $P2_1/c$. The asymmetric unit contains one H_2pdt ligand, chelating the copper atom and one iodide atom, binding terminally to the copper atom (Figure 9 a). Through the additional coordination of the symmetry related atom S1b, responsible for the growth of the one-dimensional coordination polymer along the 2_1 screw axis, the tetrahedral coordination of the Cu^I atom is completed. Important bond lengths and angles are summerized in Table SI-5. Because of the μ_2-bridging coordination of S1, its bond lengths towards copper atoms are slightly longer than that of S2 (S1–Cu1 233.6(2) pm, S1–Cu1a 239.3(2) pm, S2–Cu2 230.1(2) pm). The short S–C distances of 169.8(7) and 167.8(6) pm illustrate again the dithione character of the ligand. The chains are arranged in a zipper-like fashion, whereas one N–H proton of the ligands interact with the C_2S_2Cu units of one neighboring chain in an edge-to-face N–H···π aromatic tilted T structure (Figure 9b). The distance between a least squares plane through the C_2S_2Cu unit and the nitrogen atom bound to the interacting proton is 332.1(5) pm.

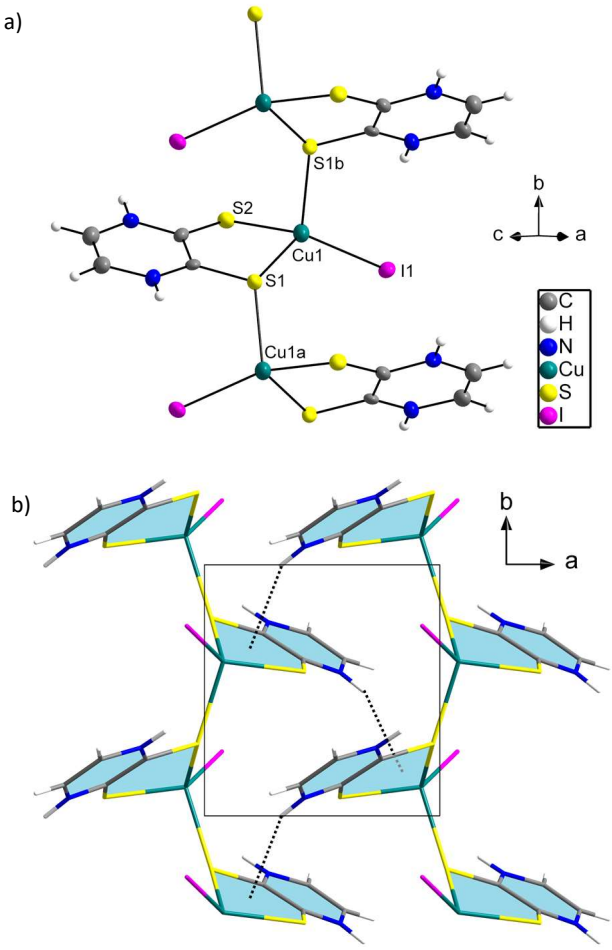

Figure 9. Ellipsoid representation (50 %) of $^{1D}[Cu(H_2pdt)I]$ (**4**) (a) and representation of the packed coordination polymer chains with edge-to-face N–H···π interaction. The view is along $[00\bar{1}]$ (b). Symmetry codes: a (2-x, -0.5+y, 0.5-z), b (2-x, 0.5+y, 0.5-z).

Table 2. Crystal and structure refinement data of **1**–**5**.[#]

	$[Cu(H_2pdt)_2]Cl$ **(1)**	$^{1D}[Ag(Hpdt)]$ **(2^{Ag})**	$^{1D}[Cu(Hpdt)]$ **(2^{Cu})**	$[Cu(Hpdt)_2]$ **(3)**	$^{1D}[Cu(H_2pdt)I]$ **(4)**	$^{1D}[Cu_2I_2(H_2pdt)(Hpdt)]$ **(5)**
Space group	$P2_1/c$	$P2_1/n$	$Pna2_1$	$P\bar{1}$	$P2_1/c$	$P\bar{1}$
a / pm	1203.76(5)	1032.38(5)	1098.96(7)	399.84(4)	647.36(4)	429.37(1)
b / pm	1444.46(4)	409.08(2)	1434.71(7)	862.76(8)	688.54(3)	1170.95(3)
c / pm	783.22(3)	1677.02(9)	415.34(2)	990.63(8)	1809.5(1)	1591.33(6)
α / °	90	90	90	64.908(6)	90	88.987(2)
β / °	90.863(3)	90.567(4)	90	82.206(7)	93.491(5)	89.165(2)
γ / °	90	90	90	79.854(7)	90	80.960(3)
V /10^6 pm^3	1361.70(9)	708.21(6)	654.86(6)	303.93(5)	805.05(8)	789.94(4)
Z	4	4	4	1	4	2
T	180 K	180 K	180 K	180 K	180 K	293 K
R_1 (I>2σ(I))	0.030	0.035[i]	0.047	0.026	0.047	R_{wp} = 4.65[*]
wR_2 (all data)	0.088	0.089[i]	0.118	0.064	0.131	R_p = 3.53[*]

[#]: Further details are provided in Tables SI-1 and SI-2.
[*]: The structure was solved and refined using X-ray powder diffraction data (Rietveld method).
[i]: The PLATON/SQUEEZE-routine[38] was applied to account for diffuse electron density in the pores (R_1 before SQUEEZE: 0.044).

$^{1D}[Cu_2I_2(H_2pdt)(Hpdt)]$ (5)

The powder diffraction pattern of **4** changes upon heating in the range of 150–190 °C and finally crystallinity is lost above 270 °C (Figure SI-3). The transformations are irreversible, as the diffraction pattern remained the same after cooling to room temperature. This indicates that a chemical reaction occured above 190 °C. Since no single crystals could be obtained, the crystal structure was solved and refined on the basis of powder X-ray diffraction data. Indexing the new phase revealed a loss in symmetry from $P2_1/c$ to $P\bar{1}$, accompanied by a change of the lattice parameters, while maintaining approximately the unit cell volume (Table 2). It was consequently assumed that the asymmetric unit has been doubled. Crystal structure solution and Rietveld refinement (Figure SI-10) show that a chainlike structure has been preserved, however, the Cu atoms are no longer bridged by a dithiolene sulfur atom. Instead, half of the copper atoms (Cu1) are bridged by iodine atoms I1 (Figure 10a). The tetrahedral coordination of Cu1 is completed by a crystallographically independent iodine atom I2 and S3, belonging to an appoximately square planar copper bis-pyrazindithiolate complex of Cu2. Assuming a formal oxidation state of +I for Cu1 and +II for Cu2, one pyrazinedithiolene ligand must be singly deprotonated. This open shell and asymmetrically protonated complex probably arose via oxidation and dehydrogenation of the ligand, like it was already described for the formation of **3**. The Cu–S distances in the formal $[Cu^{II}(H_2pdt)(Hpdt)]^+$ unit were refined to 232–235 pm. Despite the relatively large standard deviation of up to 4 pm (Table SI-9), these values appear rather long for a Cu^{II} dithiolene complex, exhibiting typical Cu–S bond lengths around 226 pm. It should be mentioned, however, that isolated Cu^{II} dithiolate complexes are usually twofold negatively charged in contrast to the herein threefold protonated, mono-cationic complex. For the Rietveld refinement, the H_2pdt and $Hpdt^-$ units were treated as rigid bodies, and C–C, C–N, and C–S bond lenghts were not freely refined. The $[Cu(H_2pdt)(Hpdt)]^+$ moieties show no significant distortion from planarity with a dihedral angle between S1/Cu2/S2 and S3/Cu2/S4 of 2(1)°. They form tilted parallel stacks along the uniform ···Cu–μ-I–Cu··· coordination bonds along the *c* axis with a distance between stacked units of 325(2)–334(4) pm (Figure 10b and 10c). The angle between the stacking axis (crystallographic *c* axis) and a least squares plane through one $[Cu(H_2pdt)(Hpdt)]^+$ moiety is 51°. The one-dimensional coordination polymer is linked to the neighbouring chain via I···H–N hydrogen bonds (I1···N1 350(1) pm, Figure 10a).

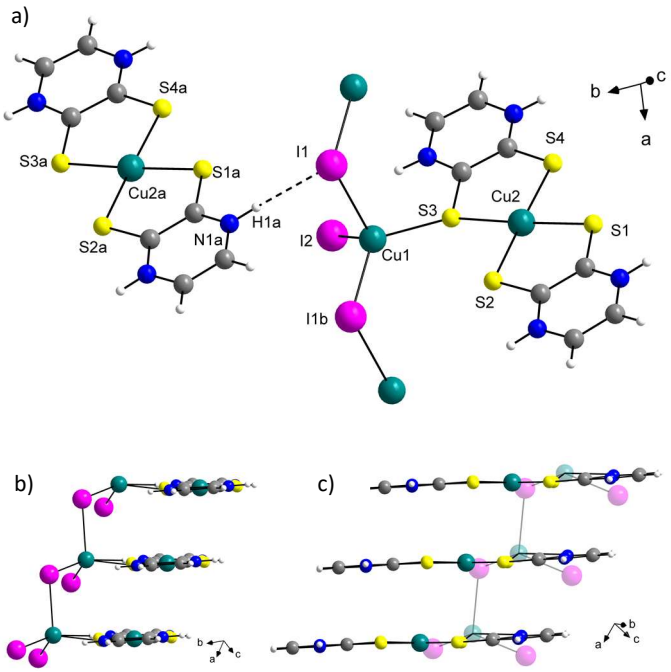

Figure 10. Ball and stick representation of $^{1D}[Cu_2I_2(H_2pdt)(Hpdt)]$ (**5**) with connectivity between two stacks (a). Two N–H hydrogen atoms are disordered with 50 % occupancy. Stack of $[Cu(H_2pdt)(Hpdt)]^+$ moieties, viewed along their long axis (b) and short axis (c). Symmetry codes: a (-1+x, 1+y, z), b (1+x, y, z).

Electronic structure of $[Cu(H_2pdt)_2]Cl$ (**1**)

As depicted in Figure 11, DFT calculations of $[Cu(H_2pdt)_2]^+$ suggest that the HOMO and the degenerate symmetry equivalent HOMO-1 consist of a σ antibonding combination of the Cu d_{xy} and the sulfur p_x and p_y orbitals with a considerable contribution of the outer carbon and nitrogen p orbitals. Oxidation of the complex with the assumed copper oxidation state of +I would, thus, mainly occur at the CuS_4 unit with a small effect on the ligand. The σ antibonding interaction in the CuS_4 core also explains the relatively long Cu–S bond lengths observed in the crystal structure of **1**. The LUMO and the degenerate symmetry equivalent LUMO+1 are composed of ligand atom p_z orbitals, which are C–C bonding, and C–N and C–S antibonding. No contribution from the metal center is observed. The ligand in **1** can, therefore, be regarded as non-innocent regarding redox reactions.

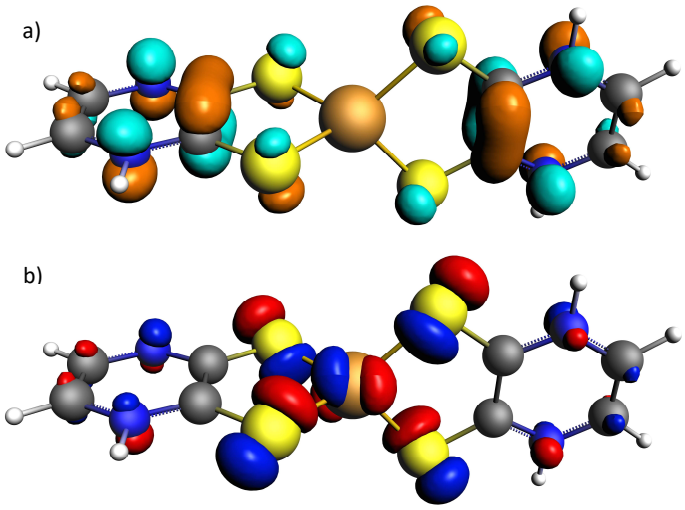

Figure 11. LUMO (a) and HOMO (b) of $[Cu(H_2pdt)_2]^+$. The LUMO is shown in orange and cyan, the HOMO is presented in blue and red to indicate the sign of the radial part of the wave function, respectively.

A special feature of **1** is its intense blue color in solutions of DMSO (dimethyl sulfoxide) and methanol. This is reflected in a strong absorption band at 600 nm ($\varepsilon = 9 \cdot 10^3$ cm^{-1} M^{-1}, Figure 12). TD-DFT simulation centers the transition with the highest oscillator strength at 626 nm. It is based on a HOMO to LUMO transition, which can be regarded as a metal-to-ligand charge-transfer (MLCT) excitation with significant contribution of the sulfur p orbitals to the electron donor orbital. (Table SI-10, Figure 11). A second strong transition at 375 nm predicted by simulation can be found in the experimental spectrum at 374 nm ($10 \cdot 10^3$ cm^{-1} M^{-1}). This HOMO-4 to LUMO transition is best described by a π-π* excitation with a small MLCT component (Figure SI-11). Whereas the absorption spectra of **1** in DMSO and methanol under inert conditions are similar in position and intensity of the absorption bands (Figure SI-12), their change upon aerial exposure is completely different. Solutions of **1** in methanol were found to be stable for about two hours, before the intensity of the absorption slowly decreases. The oxidation product, complex **3**, precipitated overnight, leaving a colorless solution. The air exposure of a DMSO solution of **1** did show an immediate effect on the solution absorption spectrum (Figure 12). While the absorption peak at 600 nm disappears, the appearance of the band at 442 nm indicates the formation of the formal Cu^{II} complex. Since the absorption spectrum of **1** after 160 minutes of air exposure perfectly matches that of compound **3** (Figure SI-13), a concurrent deprotonation process is assumed. With further air exposure, the now orange solution became pale yellow. The corresponding photometric response of this process (Figure SI-14) displays the decreasing absorption at 442 nm, as well as the emergence of a new band at 381 nm. Latter can be attributed to the formal Cu^{III} species of the complex.[29] The spectra intersect in two sets of isobestic points, indicating a constant stoichiometry and that no secondary reactions occur during the considered time range of each oxidation process.[52]

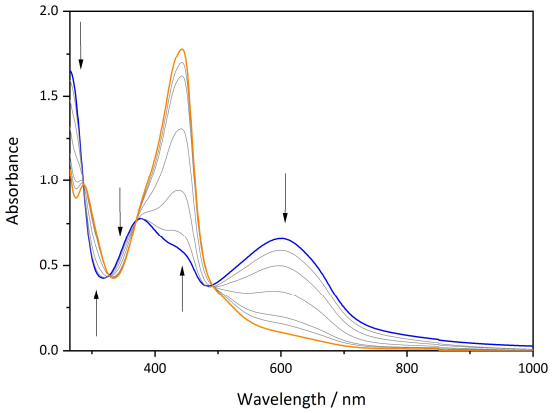

Figure 12. UV-Vis-NIR absorption spectrum of **1** in DMSO (blue) and spectral variation upon air exposure for 160 minutes (orange).

Both oxidation processes were investigated via cyclic voltammetry in DMSO. Figure 13 shows two quasi-reversible waves at low potentials, $E_{1/2}$ = -0.52 V and $E_{1/2}$ = -0.28 V vs. Fc/Fc^+. Interestingly, the fully deprotonated complex $[Cu(pdt)_2]^-$ exhibits just one reversible wave under the same conditions at $E_{1/2}$ = -0.71 V vs. Fc/Fc^+ (Figure SI-15), attributed to the Cu^{II}/Cu^{III} redox couple.[29] The fact that the two redox waves of $[Cu(H_2pdt)_2]^+$ are at far higher potentials than in $[Cu(pdt)_2]^-$ indicates that the protonation of the ligand stabilizes the reduced species. This agrees with the stability of the complex against air oxidation in methanol for several hours. The two waves recorded for **1** can be attributed to formal Cu^{I}-Cu^{II}-Cu^{III} transitions of the complex; however, as it is indicated by the distribution of the HOMO over the whole complex, the ligand p orbitals participate in the redox reaction. In comparison to typical cyclic voltammograms of dithiolene complexes the waves in Figure 13 are rather broad. Moreover, the current maxima and minima of each process are separated by around 150–170 mV (at v = 25 mV/s), increasing with higher scan rates. This is typical for a hindered electron transfer on the electrode and a quasi-reversible process.[53] The electron transfer, in this case, might be accompanied by a rearrangement of the coordination geometry and also by a deprotonation/protonation of the ligand.

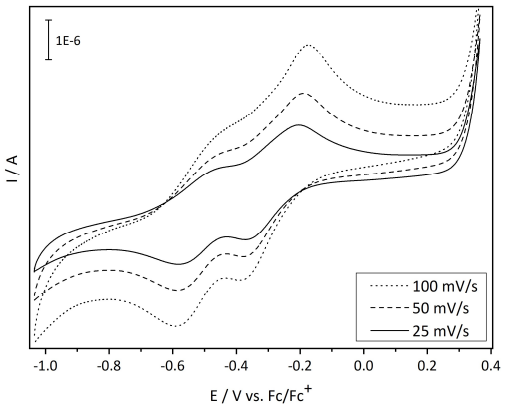

Figure 13. Cyclic voltammograms of **1** with different scan rates vs. Fc/Fc^+.

Upon scanning to potentials higher than 0.4 V vs. Fc/Fc^+, the formation of an insoluble precipitate was observed. Figure SI-16 shows two scan cycles, starting from the open circuit potential at -0.68 V in cathodic direction to -1.0 V vs. Fc/Fc^+, scanning anodically to 0.8 V vs. Fc/Fc^+, and then returning to the starting point. In the first cycle, no significant reduction current is observed below the open circuit potential. However, in the second scan, after an intense current response above 0.4 V vs. Fc/Fc^+, additional reduction processes at negative potentials (< -0.9 V vs. Fc/Fc^+) are recorded. This behavior has been observed in other dithiolene complexes[54–56] and might be explained with a chemical reaction coupled to the oxidation process. Resulting from this reaction, a product with low solubility precipitates on the surface

of the electrode. Redissolution processes take place at far lower potentials and are separated in this case by about 1.3 V.

Magnetic properties of [Cu(Hpdt)$_2$] (**3**)

The paramagnetic complex **3** was characterized by a variable temperature magnetic susceptibility measurement. As shown in Figure 14, the effective magnetic moment at 300 K is 1.77 μ_B (per formula unit) and agrees well with the expected value for isolated Cu^{2+} ions (S = ½; μ_{eff} = 1.73 μ_B, g = 2.0). Lowering the temperature, μ_{eff} decreases and reaches a value of 0.49 μ_B at 2 K. The antiferromagnetic behavior of the sample is well reflected in χ_M reaching a maximum at T_N = 6 K (Figure 14). Considering the one-dimensional stacking of Cu(II) complexes, the magnetic susceptibility was fitted with the polynomial expression derived by Hall[57] on the basis of the Heisenberg linear-chain theory for spin ½ systems from Bonner and Fisher[58].

$$\chi_M = \frac{Ng^2\beta^2}{kT} \cdot \frac{0.25 + 0.074975x + 0.07235x^2}{1.0 + 0.9931x + 0.172135x^2 + 0.757825x^3}$$

$$x = \frac{|J|}{kT}$$

The least squares fit, which is shown as red line in Figure 14, resulted in g = 2.0 and an electronic spin coupling constant of |J| = 7.3 cm^{-1}. This value is close to that obtained by the Bleaney-Bowers[59] approximation for the antiferromagnetic coupling in an assumed dimeric unit. ($|J| = k_B \cdot T \cdot 1.6 = 0.695\ cm^{-1}K^{-1} \cdot 6\ K \cdot 1.6 = 6.7\ cm^{-1}$).[60] A Curie-Weiss fit in the paramagnetic region results in a Curie constant of C = 0.40 K · emu · mol^{-1} and an asymptotic Curie temperature of Θ = -9.7 K (Figure SI-17). The antiferromagnetic behavior may be related to exchange interactions between the e^- spins of the Cu^{II} (S = ½) atoms propagated via the rather long intermolecular Cu···S interactions (324.41(7) pm). The observed magnetic behavior is in contrast to various open shell π···π stacked molecules exhibiting paramagnetic to diamagnetic phase transitions.[28,61,62] The sodium salt of the very similar Ni^{III} complex $[Ni(pdt)_2]^-$, for instance, evidences a strong antiferromagnetic interaction. This compound undergoes a phase transition between the monomeric and dimeric structure at around 220 K, similar to a spin-Peierls transition with corresponding Ni···S interactions of 371.5(1) pm (at 230 K) and 241.3(1) pm (at 210 K).[28]

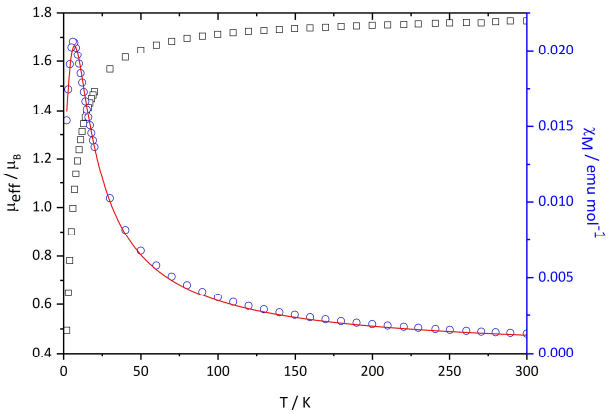

Figure 14. Temperature dependence of the effective magnetic moment μ_{eff} (black squares) and the magnetic susceptibility (blue circles) for **3** at H = 0.5 T. The red line represents the fit to the Bonner and Fisher model[58].

Electrical conductivity and band structure

Coordination polymers that exhibit electrical conductivity have attracted the interest of many researchers in materials science.[63] In this regard, materials with short Ag···Ag or Cu···Cu distances have been the subject of extensive research.[64–66] As dithiolene ligands are known to have a small orbital energy mismatch with soft Lewis acids and to participate in complex redox reactions, they are of great interest, e.g., as linker molecules for electrically conductive coordination polymers. For instance, in the three-dimensional coordination polymer Cu[Cu(pdt)$_2$] (pdt^{2-}: 2,3-pyrazinedithiolate), an electrical conductivity of 6 · 10^{-4} S/cm has been observed at room temperature.[8] Since the herein reported compounds combine dithiolene linkers with short M···M distances, the electrical properties were investigated.

Diffuse reflectance spectroscopy of **2^{Ag}**, **2^{Cu}** and **4** was performed in order to derive the optical band gaps of these materials. Assuming the scattering of the compounds independent from the wavelength, the Kubelka-Munk converted spectra can be considered as electronic absorption spectra. All compounds are intensely colored and show broad absorption maxima at 3.0 eV (**2^{Ag}**), 3.2 eV (**2^{Cu}**), and 1.9 and 2.5 eV (**4**) with shoulders to higher and lower wavelengths (Figures SI-19–21). In a first approximation, the optical band gaps were determined by extrapolating the absorption edge to the energy axis of the diffuse reflectance spectra (Kubelka-Munk function (F_{KM}), Figures SI-19–21). The resulting values are summarized in Table 3. A more elaborate way to determine optical band gaps of semiconductors is via "Tauc plots". It should be noted that Tauc plots have been developed for inorganic semiconductors and the use for coordination polymers with small band gaps and cases close to single-

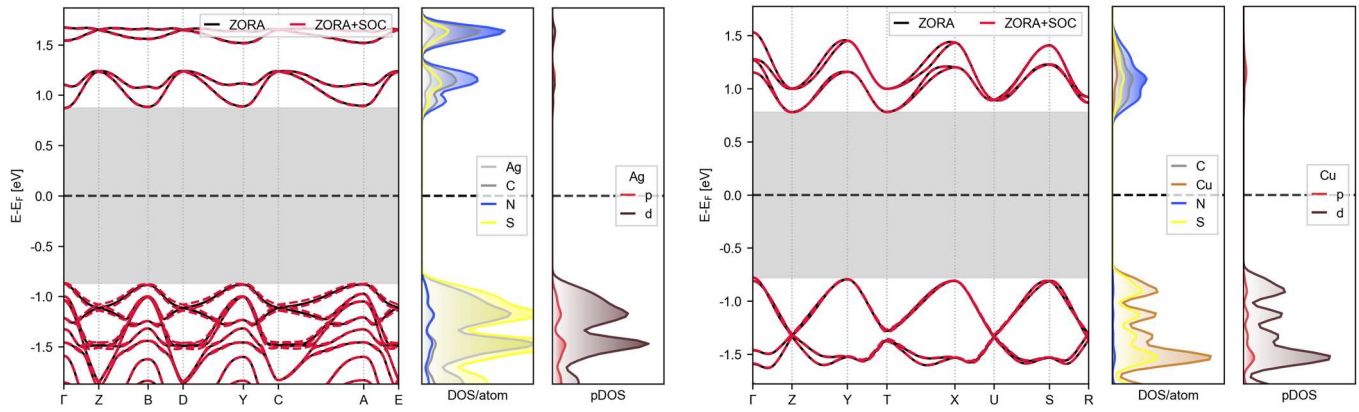

Figure 15. Band structures and projected density of states of **2^{Ag}** (left) and **2^{Cu}** (right) calculated with HSE06 including full treatment of relativistic effects through the Zeroth Order Regular Approximation (ZORA) and spin-orbit coupling (SOC).

molecule excitations must be taken with care.[67] Since DFT simulation characterized **2^{Ag}** with a direct, and **2^{Cu}** and **4** with an indirect band gap (discussion below), the graphs were plotted with η = 1/2 and 2, respectively (Figures SI-19–21). Table 3 demonstrates that both methods result in slightly different optical band gap values, with a maximum difference of 0.3 eV. In conclusion, the optical band gap of **2^{Ag}** lies in the visible region of the spectrum at about 650–590 nm, whereas electrons in **2^{Cu}** and **4** are excited at lower energies in the near infrared region at 890–1130 nm and 1380–1770 nm, respectively.

Table 3. Conductivity and band gap values for **2^{Ag}**, **2^{Cu}**, and **4**.

	$E_{g,opt}$ (F_{KM})	$E_{g,opt}$ (Tauc plot)	E_g (DFT)	Conductivity at 25 °C
2^{Ag}	1.9 eV	2.1 eV	1.74 eV	$3 \cdot 10^{-9}$ S/cm
2^{Cu}	1.4 eV	1.1 eV	1.55 eV*	$5 \cdot 10^{-6}$ S/cm
4	0.9 eV	0.7 eV	1.15 eV*	$5 \cdot 10^{-8}$ S/cm

* indirect band gap

In order to gain further insight into the electronic structure of the three one-dimensional coordination polymers, they were investigated via DFT band structure calculations, based on their X-ray diffraction structure data (Figure 15 and Figure SI-22). All three coordination polymers are confirmed to be semiconductors. While **2^{Cu}** and **4** exhibit an indirect band gap of 1.55 and 1.15 eV, **2^{Ag}** has a direct band gap of 1.74 eV (Table 3). These results corroborate the trend of decreasing optical band gaps going from **2^{Ag}** over **2^{Cu}** to **4**. While the DFT derived band gaps constitute the energy difference between the valence band maximum and the conduction band minimum, optically derived band gaps correspond to the lowest optical transition forming a bound electron hole pair (exciton). The exciton binding energy is the difference between the optically derived band gap and the electron transport gap and is usually not larger than a few tenths of an electronvolt.[68] Hence, it is not surprising that the optical band gap values of **2^{Cu}** and **4** have a smaller value than those determined by hybrid DFT calculations. The density of states analysis of the three one-dimensional coordination polymers (Figure 15 and Figure SI-22) prove a major contribution of the metal and sulfur atoms to the valence band, while the conduction band is mainly composed of the ligand carbon, nitrogen, and sulfur atom contributions. This is consistent with the presence of d^{10} metal ions (Cu^+, Ag^+) in the samples. Comparing the DOS of the two similar structures **2^{Ag}** and **2^{Cu}** (Figure 15), their major difference is that the Cu d-states spread over a larger energy range and are, thus, more delocalized and in stronger interaction with the ligand. Due to the smaller band dispersion of the **2^{Ag}** valence band, the DOS at the Fermi level is higher than in its corresponding copper analogue **2^{Cu}**.

The actual electrical conductivity of **2^{Ag}**, **2^{Cu}**, and **4** at 25 °C was measured to be $3 \cdot 10^{-9}$ S/cm, $5 \cdot 10^{-6}$ S/cm, and $5 \cdot 10^{-8}$ S/cm, respectively (Table 3). The measurements were performed on pellets using the two-probe method. As a consequence, the obtained values are probably underestimating the real conductivity due to inter-grain boundaries. Furthermore, the structures of the polymers suggest a great anisotropy of the electrical conductivity, being most likely higher within the direction of the chains. This substantial factor is not considered in the conductivity measurements of pellets. Temperature dependent experiments were performed in the range of 25–100 °C. All three investigated coordination polymers were confirmed to be semiconducting with an approximate Arrhenius temperature dependence. An Arrhenius fit to the data revealed an activation energy (E_a) of 0.15 eV for **2^{Cu}** and approx. 0.5 eV for **2^{Ag}** and **4** (Figure SI-18). For intrinsic, undoped semiconductors, the fundamental band gap is often calculated by multiplying the activation energy with the factor 2 ($E_g = 2 \cdot E_a$).[69,70] This assumption would result in thermal band gap energies of 1.0 eV for **2^{Ag}**, 0.3 eV for **2^{Cu}**, and 0.9 eV for **4**. Reproducing well the optical and DFT-determined band gaps in the case of **4**, the thermally derived band gap values for **2^{Ag}** and **2^{Cu}** are found to be of about 1 eV smaller than the corresponding optical ones. One explanation for this big difference might be the strong dependence of the electrical conductivity on the sample's purity. Any kind of impurity, defect, or dopant can significantly alter the conductivity and its temperature dependence. The linear trend of ln(σ) vs. 1/T in the region of 25–100 °C might be caused by the mechanism of extrinsic conduction, i.e., the excitation of electrons from impurity levels to the conduction band, or from valence band electrons to low lying impurity acceptor levels. Furthermore, the temperature dependent electrical conductivity measurements may be influenced, as already mentioned, by grain boundary scattering. The increase of conductivity with rising temperature might, thus, not only be due to more electrons being excited across the band gap, but also attributable to their increased kinetic energy and the consequently greater probability to overcome the boundaries.[71] In summary, the Arrhenius law to deduce band gaps might not be the most appropriate for **2^{Ag}** and **2^{Cu}**. The smaller thermal activation energy for **2^{Cu}** is, however, in accordance with its about three orders of magnitude higher electrical conductivity at room temperature.

Conclusion

Taking advantage of the dithiol-dithione tautomerism, dithiolene coordination compounds with monovalent metal ions can easily be synthesized. These materials have high potential as precursor molecules for more dimensional and conductive open-shell materials, since they are highly susceptible to proton and electron transfer reactions. As a case study, the coordination chemistry of H_2pdt towards monovalent Cu^+ and Ag^+ ions was examined. Single crystal structure analysis of H_2pdt and pK_S considerations of the sulfur and nitrogen atoms suggest that the equilibrium in solution is shifted towards the dithione tautomeric form of H_2pdt, making it an ideal ligand for soft metal ions according to the HSAB concept. From this, four new one-dimensional coordination polymers as well as two homoleptic bis(dithiolene) complexes were presented.

The coordination polymers ^{1D}[Ag(Hpdt)] (**2^{Ag}**) and ^{1D}[Cu(Hpdt)] (**2^{Cu}**) have similar structures, their metal atoms are involved in short metal···metal distances, significantly shorter than the sum of van der Waals radii. In contrast to the direct formation of **2^{Ag}**, the synthesis of its copper analogue **2^{Cu}** proceeds via the formation of a dark blue intermediate copper(I) complex, $[Cu(H_2pdt)_2]^+$. Crystal structure analysis of $[Cu(H_2pdt)_2]Cl$ (**1**) suggests that the ligand H_2pdt is present in its dithione form. Typical for the complex is its intense dark blue color in solution, caused by a strong HOMO to LUMO, MLCT, excitation. Auto-oxidation of **1** and ^{1D}[Cu(H_2pdt)I] (**4**), compounds that both bear fully protonated H_2pdt ligands, was observed upon heating. Both oxidation processes were coupled with dehydrogenation of the ligand. **1** was oxidized to the neutral copper(II) complex $[Cu(Hpdt)_2]$ (**3**), and **4** to the coordination polymer $^{1D}[Cu_2I_2(Hpdt)(H_2pdt)]$ (**5**).

Charge transport measurements revealed semiconducting behavior for **2^{Ag}**, **2^{Cu}**, and **4**. The highest conductivity and smallest activation energy was found for **2^{Cu}** and explained via DFT with widely dispersed Cu d-states.

Associated Content

Supporting Information

The Supporting Information is available free of charge at … and includes details concerning

> experimental section, crystal structure description of H_2pdt and **1'**, computational details, single crystal structure data, as well as further characterization of compounds via NMR, PXRD, temperature dependent PXRD, CV, temperature dependent conductivity measurements, variable temperature magnetic susceptibility measurements, UV-Vis-NIR spectroscopy, and diffuse reflectance spectroscopy.

Accession Codes

CCDC 2017470–2017476 contain the supplementary crystallographic data for H_2pdt and **1–5**, respectively. These data can be obtained free of charge via www.ccdc.cam.ac.uk/data_request/cif, or by emailing data_request@ccdc.cam.ac.uk, or by contacting The Cambridge Crystallographic Data Centre, 12 Union Road, Cambridge CB2 1EZ, UK; fax: + 44 1223 336033.

Author Information

Corresponding Author

Harald Krautscheid – *Institut für Anorganische Chemie, Universität Leipzig, Johannisallee 29, D-04103 Leipzig, Germany; orcid.org/0000-0002-5931-5440; Email: krautscheid@rz.uni-leipzig.de*

Authors

Stefan Henfling – *Institut für Anorganische Chemie, Universität Leipzig, Johannisallee 29, D-04103 Leipzig, Germany*

Roman Kempt – *Technische Universität Dresden, Professur für Theoretische Chemie, Bergstr. 66c, D-01062 Dresden, Germany*

Jennifer Klose – *Institut für Anorganische Chemie, Universität Leipzig, Johannisallee 29, D-04103 Leipzig, Germany*

Agnieszka Kuc – *Helmholtz-Zentrum Dresden-Rossendorf, Forschungsstelle Leipzig, Abteilung Reaktiver Transport, Institut für Ressourcenökologie, Permoserstr. 15, D-04318 Leipzig, Germany*

Berthold Kersting – *Institut für Anorganische Chemie, Universität Leipzig, Johannisallee 29, D-04103 Leipzig, Germany*

Author Contributions

All authors have given approval to the final version of the manuscript.

Funding

The work was supported by Studienstiftung des deutschen Volkes (doctoral grant for S. H.), Deutsche Forschungsgemeinschaft (DFG KR 1675/12-1, HE 3543/35-1), and BMBF (NobleNEMS). Agniszka Kuc acknowledges SFB1415 for funding.

Notes

The authors declare no competing financial interest.

Acknowledgements

We thank Dr. Oliver Kluge, Toshiki Wulf and Dr. Patrick Melix for advice concerning DFT and TD-DFT calculations and Dr. José Barzola Quiquia as well as Matthias Jakob for their help with electrical conductivity measurements. Ramona Oehme and Dr. Maik Icker with his team are acknowledged for measurements of mass and NMR spectra. The authors thank the Center for Information Services and High-Performance Computing (ZIH) at TU Dresden for generous allocations of computer time

References

(1) Stiefel, E. I., Ed. *Dithiolene Chemistry*; John Wiley & Sons, Inc, 2003. DOI: 10.1002/0471471933.

(2) Zhang, J.; Du, P.; Schneider, J.; Jarosz, P.; Eisenberg, R. Photogeneration of hydrogen from water using an integrated system based on TiO_2 and platinum(II) diimine dithiolate sensitizers. *J. Am. Chem. Soc.* **2007**, *129* (25), 7726–7727.

(3) Geary, E. A. M.; Yellowlees, L. J.; Jack, L. A.; Oswald, I. D. H.; Parsons, S.; Hirata, N.; Durrant, J. R.; Robertson, N. Synthesis, structure, and properties of Pt(II)(diimine)(dithiolate) dyes with 3,3'-, 4,4'-, and 5,5'-disubstituted bipyridyl: applications in dye-sensitized solar cells. *Inorg. Chem.* **2005**, *44* (2), 242–250.

(4) Pellaroque, A.; Noel, N. K.; Habisreutinger, S. N.; Zhang, Y.; Barlow, S.; Marder, S. R.; Snaith, H. J. Efficient and Stable Perovskite Solar Cells Using Molybdenum Tris(dithiolene)s as p-Dopants for Spiro-OMeTAD. *ACS Energy Lett.* **2017**, *2* (9), 2044–2050.

(5) Geary, E. A. M.; McCall, K. L.; Turner, A.; Murray, P. R.; McInnes, E. J. L.; Jack, L. A.; Yellowlees, L. J.; Robertson, N. Spectroscopic, electrochemical and computational study of Pt-diimine-dithiolene complexes: rationalising the properties of solar cell dyes. *Dalton Trans.* **2008** (28), 3701–3708.

(6) Islam, A.; Sugihara, H.; Hara, K.; Singh, L. P.; Katoh, R.; Yanagida, M.; Takahashi, Y.; Murata, S.; Arakawa, H.; Fujihashi, G. Dye Sensitization of Nanocrystalline Titanium Dioxide with Square Planar Platinum(II) Diimine Dithiolate Complexes. *Inorg. Chem.* **2001**, *40* (21), 5371–5380.

(7) Moorcraft, L. P.; Morandeira, A.; Durrant, J. R.; Jennings, J. R.; Peter, L. M.; Parsons, S.; Turner, A.; Yellowlees, L. J.; Robertson, N. Synthesis and properties of [Pt(4-CO_2CH_3-py)$_2$(mnt)]: comparison of pyridyl and bipyridyl-based dyes for solar cells. *Dalton Trans.* **2008** (48), 6940–6947.

(8) Takaishi, S.; Hosoda, M.; Kajiwara, T.; Miyasaka, H.; Yamashita, M.; Nakanishi, Y.; Kitagawa, Y.; Yamaguchi, K.; Kobayashi, A.; Kitagawa, H. Electroconductive porous coordination polymer Cu[Cu(pdt)$_2$] composed of donor and acceptor building units. *Inorg. Chem.* **2009**, *48* (19), 9048–9050.

(9) Robertson, N.; Cronin, L. Metal bis-1,2-dithiolene complexes in conducting or magnetic crystalline assemblies. *Coord. Chem. Rev.* **2002**, *227* (1), 93–127.

(10) Kirmse, R.; Stach, J.; Dietzsch, W.; Steimecke, G.; Hoyer, E. Single-crystal EPR studies on nickel(III), palladium(III), and platinum(III) dithiolene chelates containing the ligands isotrithionedithiolate, *o*-xylenedithiolate, and maleonitriledithiolate. *Inorg. Chem.* **1980**, *19* (9), 2679–2685.

(11) Winter, C. S.; Oliver, S. N.; Manning, R. J.; Rush, J. d.; Hill, C. A. S.; Underhill, A. E. Non-linear optical studies of nickel dithiolene complexes. *J. Mater. Chem.* **1992**, *2* (4), 443.

(12) Deplano, P.; Pilia, L.; Espa, D.; Mercuri, M. L.; Serpe, A. Square-planar d^8 metal mixed-ligand dithiolene complexes as second order nonlinear optical chromophores: Structure/property relationship. *Coord. Chem. Rev.* **2010**, *254* (13-14), 1434–1447.

(13) Kaim, W.; Schwederski, B. Non-innocent ligands in bioinorganic chemistry—An overview. *Coord. Chem. Rev.* **2010**, *254* (13-14), 1580–1588.

(14) Soricelli, C. L.; Szalai, V. A.; Burgmayer, S. J. N. Oxidation of molybdenum dithiolene complexes yields thiophene analogs of urothione and molybdopterin form B. *J. Am. Chem. Soc.* **1991**, *113* (26), 9877–9878.

(15) Solis, B. H.; Hammes-Schiffer, S. Computational study of anomalous reduction potentials for hydrogen evolution catalyzed by cobalt dithiolene complexes. *J. Am. Chem. Soc.* **2012**, *134* (37), 15253–15256.

(16) Lv, H.; Ruberu, T. P. A.; Fleischauer, V. E.; Brennessel, W. W.; Neidig, M. L.; Eisenberg, R. Catalytic light-driven generation of hydrogen from water by iron dithiolene complexes. *J. Am. Chem. Soc.* **2016**, *138* (36), 11654–11663.

(17) Gomez-Mingot, M.; Porcher, J.-P.; Todorova, T. K.; Fogeron, T.; Mellot-Draznieks, C.; Li, Y.; Fontecave, M. Bioinspired Tungsten Dithiolene Catalysts for Hydrogen Evolution: A Combined Electrochemical, Photochemical, and Computational Study. *J. Phys. Chem. B* **2015**, *119* (43), 13524–13533.

(18) Gao, S.; Fan, J.; Sun, S.; Song, F.; Peng, X.; Duan, Q.; Jiang, D.; Liang, Q. Di/mono-nuclear iron(I)/(II) complexes as functional models for the 2Fe2S subunit and distal Fe moiety of the active site of FeFe hydrogenases: protonations, molecular structures and electrochemical properties. *Dalton Trans.* **2012**, *41* (39), 12064–12074.

(19) Kennedy, S. R.; Kozar, M. N.; Yennawar, H. P.; Lear, B. J. Synthesis and characterization of the gold dithiolene monoanion, (Bu_4N)[Au(pdt = 2,3-pyrazinedithiol)$_2$]. *Polyhedron* **2016**, *103*, 100–104.

(20) Kato, R. Conducting metal dithiolene complexes: structural and electronic properties. *Chem. Rev.* **2004**, *104* (11), 5319–5346.
(21) Ray, K.; Weyhermüller, T.; Neese, F.; Wieghardt, K. Electronic structure of square planar bis(benzene-1,2-dithiolato)metal complexes $[M(L)_2]^z$ (z = 2-, 1-, 0; M = Ni, Pd, Pt, Cu, Au): an experimental, density functional, and correlated ab initio study. *Inorg. Chem.* **2005**, *44* (15), 5345–5360.
(22) Eisenberg, R.; Gray, H. B. Noninnocence in metal complexes: a dithiolene dawn. *Inorg. Chem.* **2011**, *50* (20), 9741–9751.
(23) Jørgensen, C.K. Differences between the four halide ligands, and discussion remarks on trigonal-bipyramidal complexes, on oxidation states, and on diagonal elements of one-electron energy. *Coord. Chem. Rev.* **1966**, *1* (1), 164–178.
(24) Chrysochos, N.; Ahmadi, M.; Wahlefeld, S.; Rippers, Y.; Zebger, I.; Mroginski, M. A.; Schulzke, C. Comparison of molybdenum and rhenium oxo bis-pyrazine-dithiolene complexes - in search of an alternative metal centre for molybdenum cofactor models. *Dalton Trans.* **2019**, *48* (8), 2701–2714.
(25) Kennedy, S. R.; Goyal, P.; Kozar, M. N.; Yennawar, H. P.; Hammes-Schiffer, S.; Lear, B. J. Effect of Protonation upon Electronic Coupling in the Mixed Valence and Mixed Protonated Complex, [Ni(2,3-pyrazinedithiol)$_2$]. *Inorg. Chem.* **2016**, *55* (4), 1433–1445.
(26) Kennedy, S. R.; Kozar, M. N.; Yennawar, H. P.; Lear, B. J. Steady-State Spectroscopic Analysis of Proton-Dependent Electron Transfer on Pyrazine-Appended Metal Dithiolenes [Ni(pdt)$_2$], [Pd(pdt)$_2$], and [Pt(pdt)$_2$] (pdt = 2,3-Pyrazinedithiol). *Inorg. Chem.* **2016**, *55* (17), 8459–8467.
(27) Kimura, Y.; Hayashi, M.; Yoshida, Y.; Kitagawa, H. Rational Design of Proton-Electron-Transfer System Based on Nickel Dithiolene Complexes with Pyrazine Skeletons. *Inorg. Chem.* **2019**, *58* (6), 3875–3880.
(28) Takaishi, S.; Hada, M.; Ishihara, N.; Breedlove, B. K.; Katoh, K.; Yamashita, M. Coordination mode-tuned stacking motif in alkali metal salts of Ni(pdt)$_2$ complexes (pdt = 2,3-pyrazinedithiol) and its physical properties. *Polyhedron* **2013**, *52*, 333–338.
(29) Ribas, X.; Dias, J. C.; Morgado, J.; Wurst, K.; Molins, E.; Ruiz, E.; Almeida, M.; Veciana, J.; Rovira, C. Novel Cu^{III} bis-1,2-dichalcogenene complexes with tunable 3D framework through alkaline cation coordination: a structural and theoretical study. *Chem. Eur. J.* **2004**, *10* (7), 1691–1704.
(30) Kobayashi, Y.; Jacobs, B.; Allendorf, M. D.; Long, J. R. Conductivity, Doping, and Redox Chemistry of a Microporous Dithiolene-Based Metal−Organic Framework. *Chem. Mater.* **2010**, *22* (14), 4120–4122.
(31) Rauchfuss, T. B. Synthesis of Transition Metal Dithiolenes in Dithiolene Chemistry. In *Dithiolene Chemistry*; Stiefel, E. I., Ed.; John Wiley & Sons, Inc, 2003; pp 1–54.
(32) Katritzky, A. R.; Lagowski, J. M. Prototropic Tautomerism of Heteroaromatic Compounds: II. Six-Membered Rings. In *Advances in heterocyclic chemistry*; Katritzky, A. R., Ed.; Advances in Heterocyclic Chemistry, v. 1; Academic Press, 1963; pp 339–437. DOI: 10.1016/S0065-2725(08)60529-2.
(33) Pearson, R. G. Hard and Soft Acids and Bases. *J. Am. Chem. Soc.* **1963**, *85* (22), 3533–3539.
(34) Boyde, S.; Garner, C. D.; Clegg, W. A structural comparison of bis(quinoxaline-2,3-dithiolato)cuprate complexes. *J. Chem. Soc., Dalton Trans.* **1987**, *5*, 1083.
(35) Sellmann, D.; Binder, H.; Häußinger, D.; Heinemann, F. W.; Sutter, J. Transition metal complexes with sulfur ligands: Part CXLIV. Square planar nickel complexes with NiS_4 cores in three different oxidation states: synthesis, X-ray structural and spectroscopic studies. *Inorg. Chim. Acta* **2000**, *300-302*, 829–836.
(36) Beswick, C. L.; Schulamnn, J. M.; Stiefel, E. I. Structures and Structural Trends in Homoleptic Dithiolene Complexes. In *Dithiolene Chemistry*; Stiefel, E. I., Ed.; John Wiley & Sons, Inc, 2003; pp 55–110.
(37) Colston, K. J.; Dille, S. A.; Mogesa, B.; Astashkin, A. V.; Brant, J. A.; Zeller, M.; Basu, P. Design, Synthesis, and Structure of Copper Dithione Complexes: Redox-Dependent Charge Transfer. *Eur. J. Inorg. Chem.* **2019**, *2019* (46), 4939–4948.
(38) Bondi, A. van der Waals Volumes and Radii. *J. Phys. Chem.* **1964** (68), 441–451.
(39) Spek, A. L. Single-crystal structure validation with the program PLATON. *J. Appl. Crystallogr.* **2003**, *36* (1), 7–13.
(40) Calatayud, M. L.; Castro, I.; Julve, M.; Sletten, J. Cu(II) and Cu(I) complexes with 1,2-dithiosquarate as a ligand; from molecular compounds to supramolecular network structures. *J. Mol. Struct.* **2008**, *876* (1-3), 328–338.
(41) Jansen, M. Homoatomic d^{10}-d^{10} Interactions: Their Effects on Structure and Chemical and Physical Properties. *Angew. Chem. Int. Ed.* **1987**, *26*, 1098–1110.
(42) Merz, K. M.; Hoffmann, R. d^{10}-d^{10} Interactions: multinuclear copper(I) complexes. *Inorg. Chem.* **1988**, *27* (12), 2120–2127.
(43) Cotton, F. A.; Feng, X.; Matusz, M.; Poli, R. Experimental and theoretical studies of the copper(I) and silver(I) dinuclear N,N'-di-p-tolylformamidinato complexes. *J. Am. Chem. Soc.* **1988**, *110* (21), 7077–7083.
(44) Cotton, F. A.; Feng, X.; Timmons, D. J. Further Study of Very Close Nonbonded Cu^{I}-Cu^{I} Contacts. Molecular Structure of a New Compound and Density Functional Theory Calculations. *Inorg. Chem.* **1998**, *37* (16), 4066–4069.
(45) Abraham, S. P.; Samuelson, A. G.; Chandrasekhar, J. Variations in the copper(I)-copper(I) distances in multinuclear clusters with identical coordination geometries. Short metal-metal contacts induced by oligomerization. *Inorg. Chem.* **1993**, *32* (26), 6107–6111.
(46) Pyykkö, P. Strong Closed-Shell Interactions in Inorganic Chemistry. *Chem. Rev.* **1997**, *97* (3), 597–636.
(47) Pyykkö, P.; Li, J.; Runeberg, N. Predicted ligand dependence of the Au(I)…Au(I) attraction in $(XAuPH_3)_2$. *Chemical Physics Letters* **1994**, *218* (1-2), 133–138.
(48) Mehrotra, P. K.; Hoffmann, R. Copper(I)-copper(I) interactions. Bonding relationships in d^{10}-d^{10} systems. *Inorg. Chem.* **1978**, *17* (8), 2187–2189.
(49) Knotter, D. M.; Grove, D. M.; Smeets, W. J. J.; Spek, A. L.; van Koten, G. A new class of organocopper and organocuprate compounds derived from copper(I) arenethiolates. *J. Am. Chem. Soc.* **1992**, *114* (9), 3400–3410.
(50) Schmidbaur, H.; Schier, A. A briefing on aurophilicity. *Chem. Soc. Rev.* **2008**, *37* (9), 1931–1951.
(51) Schmidbaur, H. The aurophilicity phenomenon: A decade of experimental findings, theoretical concepts and emerging applications. *Gold Bull* **2000**, *33* (1), 3–10.
(52) Nič, M.; Jirát, J.; Košata, B.; Jenkins, A.; McNaught, A. *IUPAC Compendium of Chemical Terminology*; IUPAC, 2009. DOI: 10.1351/goldbook.
(53) Hamann, C. H.; Vielstich, W. *Elektrochemie*, 4., vollständig überarbeitete und aktualisierte Auflage; Wiley-VCH-Verlag GmbJ &Co. KGaA, 2005.
(54) Hayashi, M.; Otsubo, K.; Kato, T.; Sugimoto, K.; Fujiwara, A.; Kitagawa, H. A compact planar low-energy-gap molecule with a donor-acceptor-donor nature based on a bimetal dithiolene complex. *Chem. Commun.* **2015**, *51* (87), 15796–15799.
(55) Tommasino, J.-B.; Pomarede, B.; d. Medus; Montauzon, D. de; Cassoux, P.; Fabre, P.-L. Electrochemical Studies of the Formation Mechanism of $(cation)_x[Ni(dmit)_2]$ Conductive Compounds and of their Non-Integer Oxidation State. *Mol. Cryst. Liq. Cryst. Sci. Technol., Sect. A* **1993**, *237* (1), 445–456.
(56) Pullen, A. E.; Olk, R.-M.; Zeltner, S.; Hoyer, E.; Abboud, K. A.; Reynolds, J. R. A New Generation of Nickel−dmit-Based Molecular Conductors Based on Fully Conjugated Bimetallic Complexes. *Inorg. Chem.* **1997**, *36* (6), 958–959.
(57) Hatfield, W. E.; Weller, R. R.; Hall, J. W. Exchange coupling in the sulfur-bridged quasi-linear-chain compound bis(dimethyldithiocarbamato)copper(II). Observations on exchange in sulfur-bridged copper(II) compounds. *Inorg. Chem.* **1980**, *19* (12), 3825–3828.
(58) Bonner, J. C.; Fisher, M. E. Linear Magnetic Chains with Anisotropic Coupling. *Phys. Rev.* **1964**, *135* (3A), A640-A658.

(59) Bleaney, B.; Bowers, K. D. Anomalous paramagnetism of copper acetate. *Proc. R. Soc. Lond. A* **1952**, *214* (1119), 451–465.
(60) Gade, L. H. *Koordinationschemie*, 1. Auflage; Wiley-VCH, 1998. DOI: 10.1002/9783527663927.
(61) Brusso, J. L.; Clements, O. P.; Haddon, R. C.; Itkis, M. E.; Leitch, A. A.; Oakley, R. T.; Reed, R. W.; Richardson, J. F. Bistabilities in 1,3,2-dithiazolyl radicals. *J. Am. Chem. Soc.* **2004**, *126* (26), 8256–8265.
(62) Umezono, Y.; Fujita, W.; Awaga, K. Coordination bond formation at charge-transfer phase transition in $(BDTA)_2[Co(mnt)_2]$. *J. Am. Chem. Soc.* **2006**, *128* (4), 1084–1085.
(63) Givaja, G.; Amo-Ochoa, P.; Gómez-García, C. J.; Zamora, F. Electrical conductive coordination polymers. *Chem. Soc. Rev.* **2012**, *41* (1), 115–147.
(64) Delgado, S.; Sanz Miguel, P. J.; Priego, J. L.; Jiménez-Aparicio, R.; Gómez-García, C. J.; Zamora, F. A conducting coordination polymer based on assembled Cu_9 cages. *Inorg. Chem.* **2008**, *47* (20), 9128–9130.
(65) Sun, D.; Cao, R.; Weng, J.; Hong, M.; Liang, Y. A novel luminescent 3D polymer containing silver chains formed by ligand unsupported Ag–Ag interactions and organic spacers. *J. Chem. Soc., Dalton Trans.* **2002**, *39* (3), 291.
(66) Su, W.; Hong, M.; Weng, J.; Cao, R.; Lu, S. A Semiconducting Lamella Polymer $[\{Ag(C_5H_4NS)\}_n]$ with a Graphite-Like Array of Silver(I) Ions and Its Analogue with a Layered Structure. *Angew. Chem. Int. Ed.* **2000**, *39* (16), 2911–2914.
(67) Sippel, P.; Denysenko, D.; Loidl, A.; Lunkenheimer, P.; Sastre, G.; Volkmer, D. Dielectric Relaxation Processes, Electronic Structure, and Band Gap Engineering of MFU-4-type Metal-Organic Frameworks:Towards a Rational Design of Semiconducting Microporous Materials. *Adv. Funct. Mater.* **2014**, *24* (25), 3885–3896.
(68) Bredas, J.-L. Mind the gap! *Mater. Horiz.* **2014**, *1* (1), 17–19.
(69) Sun, L.; Campbell, M. G.; Dincă, M. Electrically Conductive Porous Metal-Organic Frameworks. *Angew. Chem. Int. Ed.* **2016**, *55* (11), 3566–3579.
(70) Michel, C.; Baranovskii, S. D.; Klar, P. J.; Thomas, P.; Goldlücke, B. Strong non-Arrhenius temperature dependence of the resistivity in the regime of traditional band transport. *Appl. Phys. Lett.* **2006**, *89* (11), 112116.
(71) Gándara, F.; Uribe-Romo, F. J.; Britt, D. K.; Furukawa, H.; Lei, L.; Cheng, R.; Duan, X.; O'Keeffe, M.; Yaghi, O. M. Porous, Conductive Metal-Triazolates and Their Structural Elucidation by the Charge-Flipping Method. *Chem. Eur. J.* **2012**, *18* (34), 10595–10601.

For Table of Contents Only

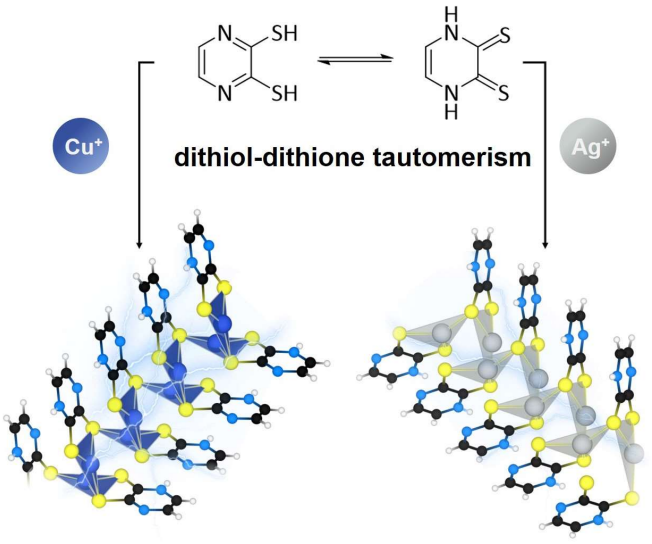

Based on the dithiol-dithione tautomerism of 2,3-pyrazinedithiol, we present the synthesis and characterization of two mononuclear complexes as well as four one-dimensional coordination polymers with silver and copper atoms. Two of them exhibit short metal···metal distances and their electronic properties were investigated. Open shell species were formed upon heating of the compounds that bear fully protonated ligands. The auto-oxidation was found to be coupled with a dehydrogenation of the pyrazine unit.